Journal of Nuclear Materials 393 (2009) 235–241

Contents lists available at ScienceDirect

Journal of Nuclear Materials

journal homepage: www.elsevier.com/locate/jnucmat

Microstructural analysis of an HT9 fuel assembly duct irradiated in FFTF to 155 dpa at 443 °C

B.H. Sencer [a,*], J.R. Kennedy [a], J.I. Cole [a], S.A. Maloy [b], F.A. Garner [c]

[a] Idaho National Laboratory, Idaho Falls, ID 83415, USA
[b] Los Alamos National Laboratory, Los Alamos, NM 87545, USA
[c] Radiation Effects Consulting, Richland, WA 99352, USA

ARTICLE INFO

Article history:
Received 24 February 2009
Accepted 11 June 2009

ABSTRACT

The majority of data on the irradiation response of ferritic/martensitic steels has been derived from simple free-standing specimens irradiated in experimental assemblies under well-defined and near-constant conditions, while components of long-lived fuel assemblies are more complex in shape and will experience progressive changes in environmental conditions. To explore whether the resistance of HT9 to void swelling is maintained under more realistic operating conditions, the radiation-induced microstructure of an HT9 ferritic/martensitic hexagonal duct was examined following a six-year irradiation of a fuel assembly in the Fast Flux Test Reactor Facility (FFTF). The calculated irradiation exposure and average operating temperature of the duct at the location examined were ~155 dpa at ~443 °C. It was found that dislocation networks were predominantly composed of (a/2)<1 1 1> Burgers vectors. Surprisingly, for such a large irradiation dose, type a<1 0 0> interstitial loops were observed. Additionally, a high density of precipitation occurred. These two microstructural characteristics may have contributed to the rather low swelling level of 0.3%.

Published by Elsevier B.V.

1. Introduction

Ferritic-martensitic steels provide attractive alternatives to the use of austenitic stainless steels for fission, fusion, spallation and fast reactor applications. This is in part a consequence of their generally greater resistance to neutron irradiation-induced swelling and creep and their reasonably acceptable high temperature strength [1–12], although these attributes are somewhat sensitive to alloy composition and processing history.

The ferritic-martensitic alloy HT9 has been investigated in the USA for application to fast, fusion and spallation neutron driven devices. This alloy has shown great promise, especially with respect to its resistance to swelling and excellent compatibility with sodium. To date, however, all reported swelling and creep data on this alloy have been derived from very simple, free-standing experimental specimens irradiated under rather well-defined conditions in material test assemblies [13–23].

It is known that the swelling of austenitic stainless steels is sensitive to "history effects" such that materials subjected to reactor-relevant changes in neutron flux, temperature and stress state often reach much higher swelling levels than is reached in identical material irradiated under constant irradiation conditions [24].

In order to confirm that HT9 does also not lose a large fraction of its swelling resistance under the variable irradiation conditions characteristic of long-term operation of a relatively complex component in reactor, it was decided to examine a fuel assembly from the FFTF fast reactor that employed this alloy for fuel pin cladding, wire wrap and the hexagonal duct that encased the fuel pin assembly.

This fuel assembly was designated ACO-3 and reached a maximum exposure of 155 dpa. This first published report on this duct addresses the swelling and associated microstructure of the duct at the position of maximum displacement dose.

2. Experimental details

The composition of HT9 (heat 84425) used to construct the ACO-3 hexagonal duct is given in Table 1. The duct was subjected to a heat treatment involving 1038 °C/5 min/air cooling followed by 760 °C/30 min/air cool. The duct was 367 cm long (12 ft), hexagonal in cross section with a span of 60 mm across each face and a wall thickness of 3.0 mm.

The ACO-3 assembly was included in a partial core loading of FFTF known as the Core Demonstration Experiment (CDE) that was designed to be an aggressive demonstration of a fuel system using HT9 for cladding, wrapping wire and duct [25] for fuel assemblies, lead fuel assemblies and reflector assemblies. The fuel cladding started irradiation at peak cladding temperatures as high as 660 °C in some subassemblies and to maintain operation at this high temperature the CDE ensemble was progressively moved

* Corresponding author. Tel.: +1 208 533 8019; fax: +1 208 533 7863.
E-mail address: Bulent.Sencer@inl.gov (B.H. Sencer).

0022-3115/$ - see front matter Published by Elsevier B.V.
doi:10.1016/j.jnucmat.2009.06.010

Table 1
Chemical composition of HT9 in wt%.

	Fe	Cr	Ni	Mo	Mn	C	Ti	V	W	Si	Al
HT9*	bal.	11.8	0.51	1.03	0.50	0.21	<0.01	0.33	0.24	0.21	0.03

* Heat 84425, with $S = 0.003$, $P = 0.008$, $N = 0.006$.

inward in the FFTF core as burn-down of the fuel progressed [26,27]. Thus there were both slowly declining and abruptly increasing changes in both neutron flux and temperature. In general the pressure differences across the duct wall and thereby the applied stresses were low enough to be ignored.

As shown in Fig. 1 and Table 2 the ACO-3 subassembly was one of the CDE assemblies and was irradiated in three positions of the FFTF fast reactor during cycles 7 to 12B, accumulating an exposure of 1524.2 equivalent full power days (EFPD) over a six-year period, as shown in Table 3. The first position was in row 6, and the second and third positions were in row 3 in equivalent positions but on opposite sides of the core.

The fuel in the subassembly reached a peak fast fluence of 38.9×10^{26} n/m^2, $E > 0.1$ MeV. In each core position the same duct face of the ACO-3 assembly was always oriented towards the core center. During cycles 7 and 8, the reactor ran at 400 MW_{th} while in the remaining irradiation cycles, the reactor operated at 291 MW_{th}. Therefore the integrated history of the duct experienced a range of exposure conditions over a six-year period, providing a good test of the swelling resistance of HT9 under realistic operating conditions.

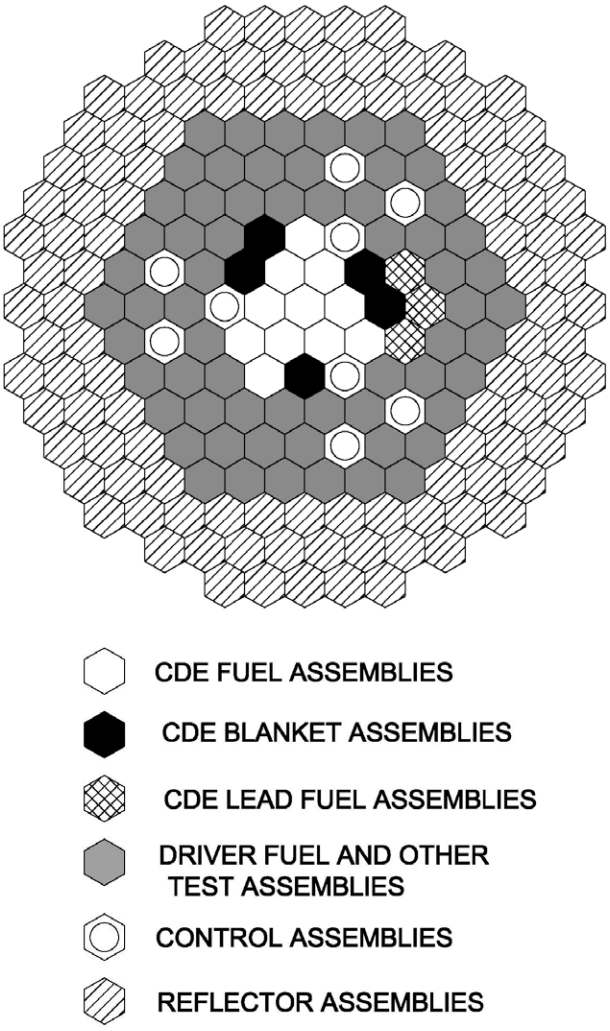

Fig. 1. Initial core loading of CDE sub-core in FFTF [25].

Estimated dose and temperature profiles at the conclusion of the ACO-3 irradiation are shown in Fig. 2. The conversion factors used to calculate dose from fast fluence were taken from analyses performed on dosimetry packets from Materials Open Test Assemblies (MOTA) located in comparable positions in the FFTF core. In the central core region, where the specimens extracted for this study were located, the conversion factors ranged between 4.1 and 4.5 dpa per 10^{26} n/m^2($E > 0.1$ MeV), depending on the core

Table 2
Irradiation dates and subassembly location of the ACO-3 duct irradiated in FFTF.

Irradiation cycle	Cycle segment	Irradiation dates	In core location code	Relative position in core	Handling socket orientation mark
7	7A	8/17/85-12/07/85	1609	Periphery	Towards core center
	7B	12/09/85-12/13/85	1609	Periphery	Towards core center
	7C	12/16/85-1/03/85	1609	Periphery	Towards core center
8A	8A	2/06/85-4/25/86	1609	Periphery	Towards core center
9A	9A.1	9/10/86-10/13/86	1304	Near center	Towards core center
	9A.2	10/16/86-2/05/86	1304	Near center	Towards core center
9B	9B	3/04/87-6/20/87	1304	Near center	Towards core center
9C	9C	7/02/87-10/10/87	1304	Near center	Towards core center
10A	10A.1	11/18/87-1/26/88	1304	Near center	Towards core center
	10A.2	2/01/88-2/23/88	1304	Near center	Towards core center
	10A.3	1/25/88-3/04/88	1304	Near center	Towards core center
	10A.4	3/07/88-5/08/88	1304	Near center	Towards core center
10B	10B	6/11/88-10/17/88	1304	Near center	Towards core center
10C	10C.1	11/09/88-1/08/89	3303	Near center	Towards core center
	10C.2	1/16/89-1/20/89	3303	Near center	Towards core center
	10C.3	1/24/89-3/13/89	3303	Near center	Towards core center
11A	11A.1	5/03/89-5/16/89	3303	Near center	Towards core center
	11A.2	5/21/89-6/02/89	3303	Near center	Towards core center
	11A.3	6/14/89-9/18/89	3303	Near center	Towards core center
11B.1	11B.1	1/04/90-4/08/90	3303	Near center	Towards core center
11B.2	11B.2	5/29/90-10/27/90	3303	Near center	Towards core center
11C	11C	12/20/90-3/19/91	3303	Near center	Towards core center
12A	12A.1	5/27/91-7/21/91	3303	Near center	Towards core center
	12A.2	7/30/91-9/22/91	3303	Near center	Towards core center
12B	12B.1	11/21/91-1/15/92	3303	Near center	Towards core center
	12B.2	1/26/92-3/19/92	3303	Near center	Towards core center

Table 3
Incremental and Cumulative EFPD for the ACO-3 duct irradiated in FFTF.

Irradiation cycle	Cycle segment	Incremental EFPD	Cumulative EFPD
7	7A	105.1	105.1
	7B	3.3	108.4
	7C	14.4	122.8
8A	8A	54.9	177.7
9A	9A.1	29.4	207.1
	9A.2	108.3	315.4
9B	9B	106.4	421.8
9C	9C	97.7	519.5
10A	10A.1	66.3	585.8
	10A.2	20.3	606.1
	10A.3	5.8	611.9
	10A.4	59.4	671.3
10B	10B	126.7	798.0
10C	10C.1	56.9	854.9
	10C.2	2.9	857.8
	10C.3	47.0	904.8
11A	11A.1	11.3	916.1
	11A.2	10.5	926.6
	11A.3	94.6	1021.2
11B.1	11B.1	85.5	1106.7
11B.2	11B.2	132.7	1239.4
11C	11C	81.5	1320.9
12A	12A.1	52.8	1373.7
	12A.2	48.6	1422.3
12B	12B.1	50.3	1472.6
	12B.2	51.6	1524.2

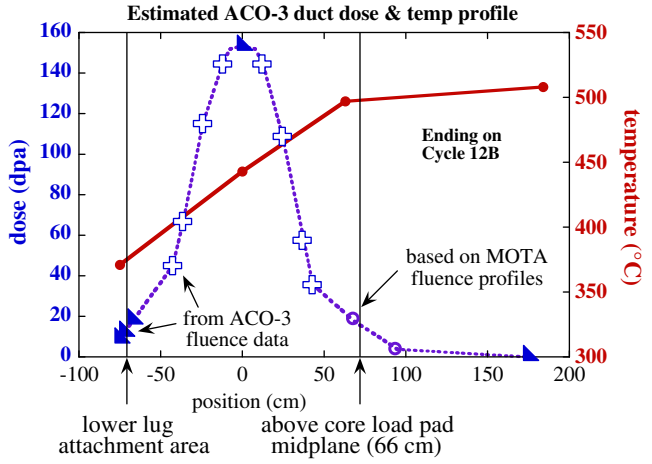

Fig. 2. Irradiation conditions that were experienced by the ACO-3 duct. Determination of dose levels was augmented using dosimetry measurements conducted in Materials Open Test Assemblies (MOTA) irradiated in comparable positions in FFTF.

power level, the local flux distribution and the surrounding assemblies in each core loading.

As shown in Fig. 2 the total dose attained in the mid-core region was ~155 dpa. Microstructural examination was conducted on a specimen located at the core center plane, which experienced the maximum neutron exposure at a time-averaged temperature of ~443 °C. Both sides of the duct face were in contact with flowing sodium and the temperature gradient across the duct was estimated to be less than 5 °C. While the displacement dose is considered to be accurate within ±5%, the variations in temperature over the lifetime have not yet been estimated. Since this component is a duct, however, the variations in temperature are probably within ±10 °C, a situation quite different from that of the fuel cladding where the temperatures are driven by the instantaneous local fission rate.

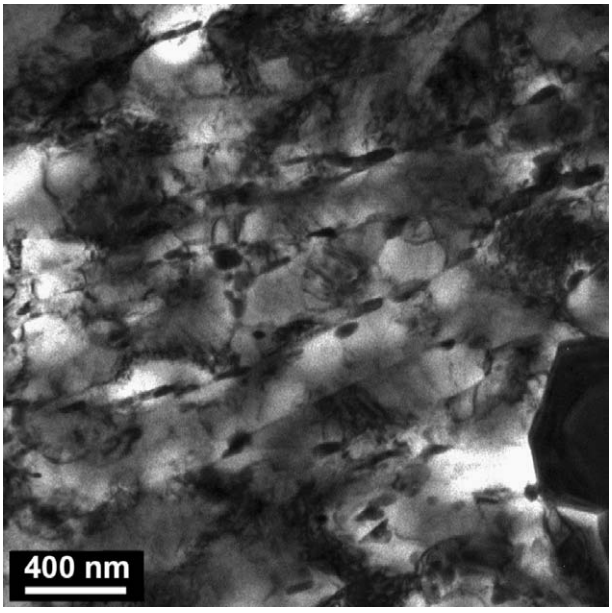

Fig. 3. Microstructure of HT9 alloy prior to neutron irradiation. The martensite transformation has occurred and carbides have formed during tempering.

The microscopy specimens used in this study were prepared by punching 2.3 mm discs. TEM samples were prepared by conventional jet electropolishing methods, in 5% perchloric acid, 95% methanol, at −40 °C and 65 A. TEM examinations were conducted with JEOL 2010 and TECHNAI G^2 F30 electron microscopes. An unirradiated archive duct was available to determine the starting microstructure.

3. Results

3.1. Preirradiation microstructure of HT9

Prior to irradiation the microstructure of unirradiated HT9 contains a duplex structure of martensite and ferrite. Large blocky carbides with a strong contrast in bright-field images were observed on the martensite lath boundaries. Carbides distributed on or near sub-grain boundaries are shown in Fig. 3.

3.2. Irradiated HT9

Detailed analysis of the microstructure examination revealed that dislocation loop, network dislocations, precipitates and cavities had developed in the HT9 alloy irradiated at 443 °C to 155 dpa with well developed precipitate arrays decorating sub-grain lath boundaries, non-uniform void arrays within laths and fine precipitates on boundaries and within laths in Fig. 4a. In addition to the small fine precipitation, large bulky carbides with strong contrast in bright-field images were observed on grain and lath boundaries as seen in Fig. 4b. It also appears, comparing Fig. 3 and Fig. 4b, that there is an enhancement in carbide density on or near the sub-grain boundaries after irradiation. The HT9 developed void structures typical of martensitic steels. These void structures consisted of void arrays between lath boundaries and void free regions on, and adjacent to, the boundaries.

In the dislocation analysis, it is assumed that the network dislocations contain only a<1 0 0> and (a/2)<1 1 1> components. Network segments in 2 0 0 dark-field image are not observable in 0 1 1 image, while another population of a<1 0 0> dislocations is imaged. Hence most must be a<1 0 0> dislocations. Weakly imaged

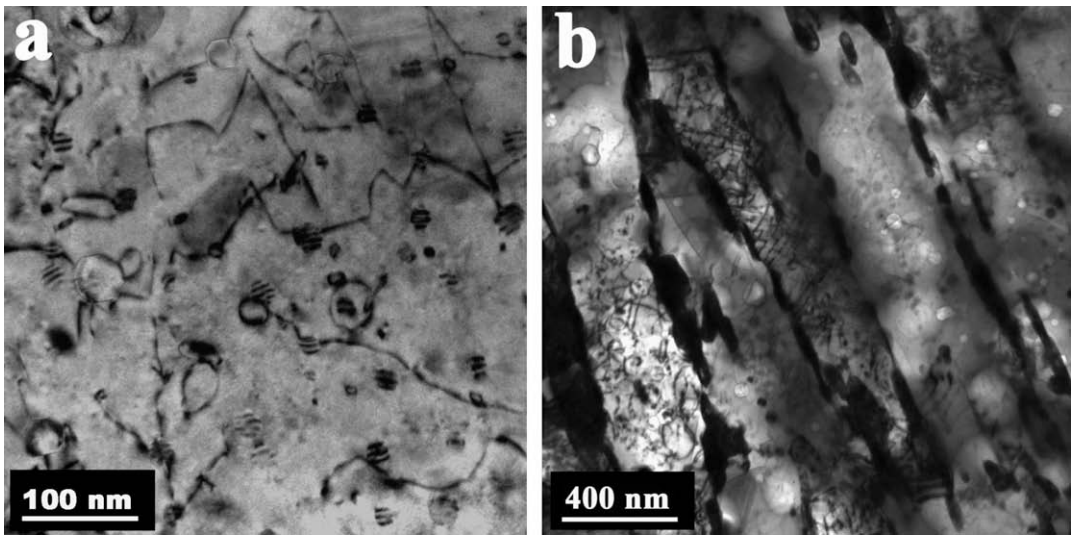

Fig. 4. (a) TEM image showing dislocation loop, network dislocations, precipitates and cavities, g = 110. (b) TEM image showing carbides on lath boundaries.

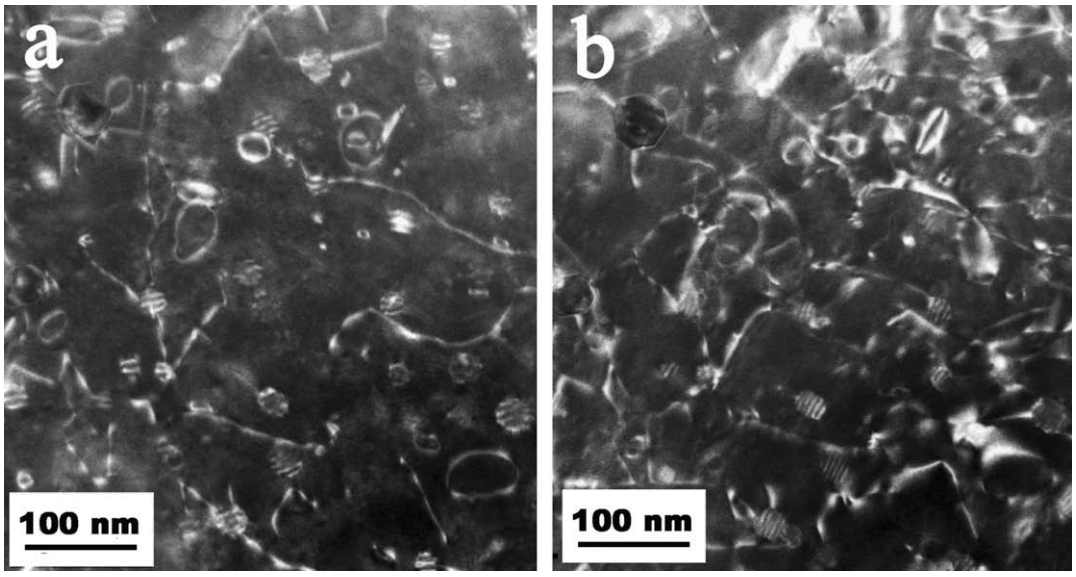

Fig. 5. TEM dark-field images of (a) g = 110 and (b) g = 200 are from the same region in irradiated HT9 at 155 dpa.

dislocations in 2 0 0 contrast are mostly (a/2)<1 1 1> dislocations, since they are also visible in 1 1 0 contrast, as seen in Fig. 5a and b. In these dark-field images the electron beam is $z = <0\ 0\ 1>$ zone. Dislocation pinning at cavity surfaces is often observed. The 200 contrast reveals 1/3 of a<1 0 0> dislocations and all of (a/2)<1 1 1> dislocations, while the 110 contrast images 2/3 of a<1 0 0> dislocations and 1/2 of (a/2)<1 1 1> dislocations. Therefore, the density of each type of dislocation is calculated from the quantification results of a pair of 2 0 0 and 1 1 0 micrographs. The total network dislocation density ((a/2)<1 1 1> + a<1 0 0>) is estimated to be $\sim 3 \times 10^{15}$ m^{-2} and (a/2)<1 1 1> dislocation density is estimated to be $\sim 2.2 \times 10^{15}$ m^{-2} indicating the network dislocation structure is predominantly (a/2)<1 1 1> type. In Fig. 5, loops are predominantly a<1 0 0> type, but their number density is relatively low. Fig. 6 also shows loops, presented together with the loop size distribution. The mean loop size is estimated to be ~18 nm. Loop number density is estimated to be $\sim 5 \times 10^{20}$ m^{-3}.

Another feature found in the microstructure of irradiated HT9, as shown in Fig. 7, is radiation enhanced precipitation that has previously been identified as G-phase by Gelles and Thomas [28] or as η phase by Maziasz and Klueh [29] and α' precipitates [4,15,16]. Fig. 8a shows a bright-field TEM image of G-phase and α' precipitates while Fig. 8b shows the precipitate dark-field image of G-phase. Comparison of Fig. 8a and b reveals that not all precipitates are imaged in Fig. 8a. The smaller precipitates do not appear in Fig. 8b are expected to be chromium rich α' precipitates. The mean G-phase precipitate size is ~20 nm in diameter within the laths, but somewhat larger on sub-grain boundaries. Irradiation hardening found in HT9 can be partially attributed to this phase. The α' precipitates have a cube-on-cube relationship with the matrix and form by precipitation of chromium with the same body centered cubic structure as the matrix and only a slightly larger (<1%) lattice constant. Hence α' precipitates can only be imaged in bright-field TEM images.

Cavities thought to be voids are shown in Fig. 9 at 155 dpa with a mean cavity size of ~28 nm. The highest swelling was measured as high as 1.2% in isolated regions. Estimated mean void swelling is ~0.3%, based on a measured cavity number density of $\sim 2.5 \times 10^{20}$ m^{-3}. Void swelling measurements were conducted as recommended in Ref. [30]. The spatial distribution of cavities was

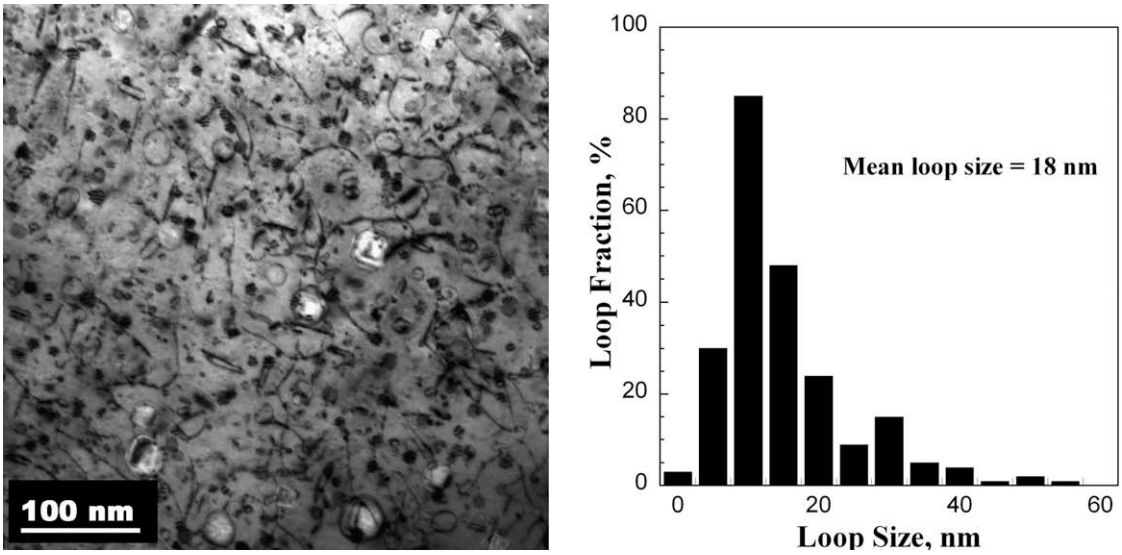

Fig. 6. Bright-field TEM image ($g = 110$) showing dislocations, small and large loops, precipitates and voids, together with loop size distribution.

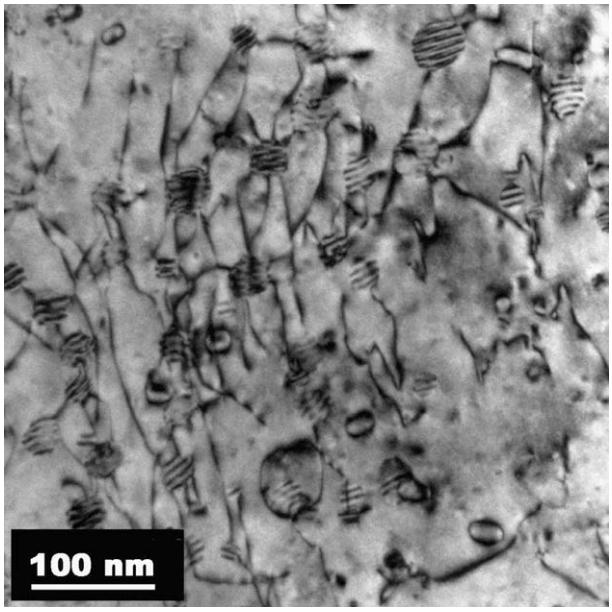

Fig. 7. Bright-field TEM image, g = 110, of both G-phase and chromium rich α' precipitates.

quite uniform within the matrix, although grain boundaries and adjacent regions were usually free of cavity formation. Since void size distribution extended to small sizes, steady-state void populations had at best only just been achieved. In some cases, voids were in linear arrays, indicating that heterogeneous nucleation on dislocations may have played a role.

4. Discussion

It is clear that even under non-constant irradiation conditions the alloy HT9 displays a remarkable resistance to void swelling. While the crystal structure of BCC iron and iron-based ferritic alloys is thought to convey immunity against the high swelling rates characteristic of FCC iron-base alloys [4], it has been shown that under some conditions (e.g., cold-working, low dpa rates) pure iron can develop relatively high swelling rates [31–33].

More importantly, the Fe–12Cr binary alloy from which HT9 is based has been shown to swell at a steady-state rate of ~0.2%/dpa [34] where data have been generated to doses as high as 30 dpa in DFR [35], 50–100 dpa in EBR-II [36] and 140–200 dpa in FFTF [37,38]. The onset of swelling of Fe–12Cr has also been shown to be accelerated by lower temperatures, lower dpa rates and carbon addition (at least at some higher temperatures) [34]. It has also been demonstrated that HT9 and 9Cr–1Mo appear to be swelling at rates comparable to that of pure binary alloys Fe–12Cr and Fe–9Cr, but to begin swelling after a somewhat longer transient regime [34]. The onset swelling of HT9 in FFTF was observed to be accelerated by application of stress [20,34]. It also appears that the swelling of Fe–Cr binary alloys is sensitive to the helium/dpa ratio [39].

It should be noted that most measurements of swelling of HT9 cited earlier were determined from either diameter changes of zero-stress creep tubes or from density change measurements. This observation is significant in that both diameter change and density change contain contributions from phase changes. These previous studies have shown however, that the combined swelling and phase-related density change behavior of HT9 is somewhat sensitive to heat-to-heat variability, minor compositional changes as well as to irradiation temperature and dpa rate.

Actual measurements of void volume *per se* were made only in references 14, 16 and 20. Most significantly, if we ignore the difference between the two specimens the current measurement of 0.3% swelling at 155 dpa and 443 °C and the stress-free swelling of ~1% at 208 dpa and ~400 °C [20,34], the swelling rate is beginning to approach the anticipated 0.2%/dpa rate, at least in the 400–450 °C temperature range. The acceleration of swelling at 208 dpa by stress from ~1% to ~2.5% [20] indicates that the swelling rate is obviously beginning to further increase, implying that the terminal rate of ~0.2%/dpa may have been reached at a dose level below 208 dpa.

From the current study alone it can not be stated confidently whether the observed swelling of 0.3% still lies in the transient regime of swelling. It may be noted that a broad void size distribution which includes small sizes is usually an indication that steady-state swelling has not been achieved. Most importantly, the somewhat complex temperature and flux history over its six-year lifetime did not appear to significantly impact the swelling resistance of the HT9 duct.

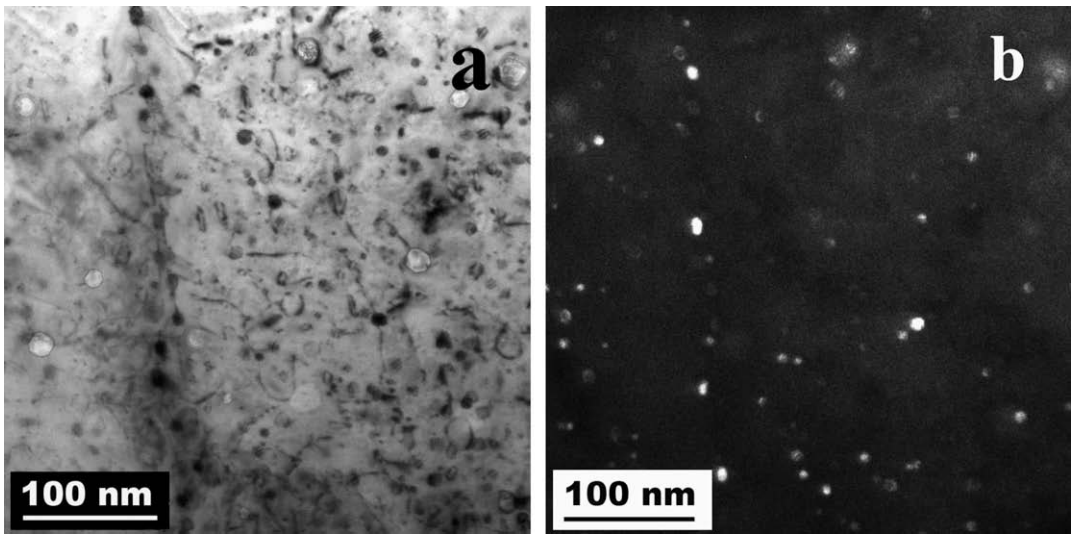

Fig. 8. (a) Bright-field TEM image of both G-phase and chromium rich α' precipitates, near void imaging condition (b) Precipitate dark-field TEM image of G-phase.

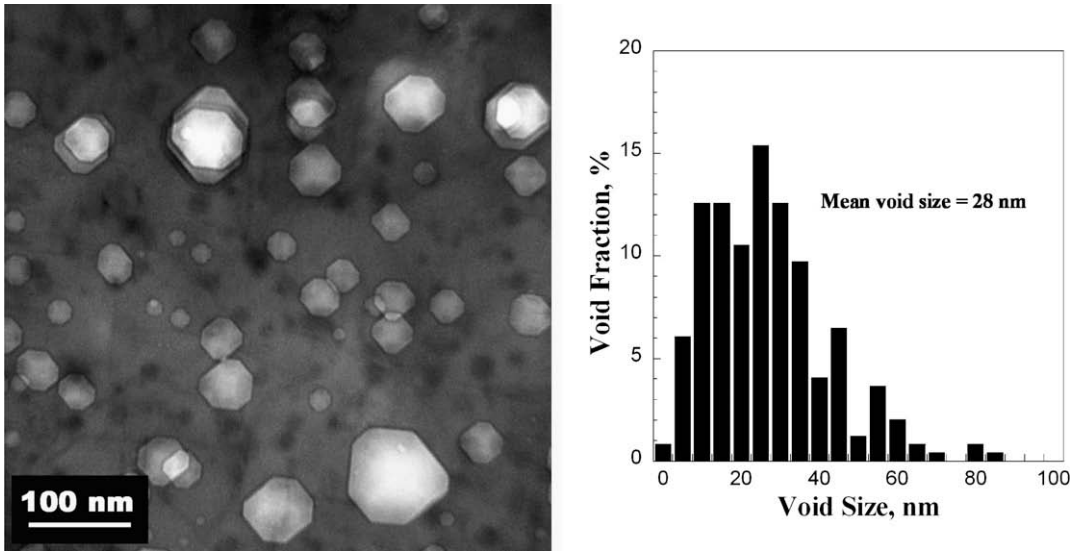

Fig. 9. TEM void image and void size distribution.

How might the exceptional swelling resistance of HT9 arise in FFTF? Most likely there are a number of factors, both environmental and material in nature. In high-flux reactors such as FFTF it is suspected that the transient regime of swelling for Fe–Cr alloys is extended at higher dpa rates as was demonstrated in comparison of swelling in FFTF and lower flux EBR-II [34]. This effect of higher dpa rate to delay the onset of steady-state swelling is well established for Fe–Cr–Ni FCC alloys [40–44] but only one study confirms that a similar phenomenon occurs in BCC iron-base alloys such as EP-450 [44].

Additionally, the higher flux reactors frequently have mixed oxide fuels rather than metal fuels. As a consequence, the neutron spectra are softened and the He/dpa ratio is reduced in oxide cores, making void nucleation more difficult [39]. Also, as noted earlier the duct in FFTF did not experience any significant stresses.

Additionally, there are some microstructural features that may contribute to the swelling resistance of HT9. Two features stand out at present. These are the nature of the precipitate evolution and that of the dislocation/loop population produced by irradiation.

The HT9 ferritic/martensitic alloy developed a high density of small precipitates which were identified to be G-phase and chromium rich α' consistent with previously published results [15,16]. The α' precipitates are typically of spheroidal geometry and in a size range resolvable by electron microscopy. If they are assumed to act like a perfect sink which would have very high point defect capture efficiency and can absorb a number of point defects of either kind, hence they would be a strong swelling suppressor. However, since α' is cube-on-cube precipitation of chromium with the same body centered cubic structure as the matrix and only a slightly larger (<1%) lattice constant, they are unlikely to be very effective sinks. Future work on the precipitations remains to be explored.

The other microstructural feature is the presence of predominantly a<1 0 0> type interstitial dislocation loops. The interstitial loops are sensitive to chromium content [16]. The presence of a

high density of such loops at this high dose is rather surprising, especially in the presence of a dislocation network. Also point defects are highly mobile at 443 °C and the possibility of interstitial clustering is extremely weak. Perhaps there is some interaction between continuous nucleation of interstitial loops and the precipitations that promotes the loop nucleation and/or stabilizes the nucleated loops. This could be supported by the coincidence of conditions for high density loop development and precipitation, especially chromium rich α' precipitates.

5. Conclusions

An HT9 duct was irradiated in three positions in FFTF over six-years at ~443 °C reaching ~155 dpa, The duct experienced both slowly declining and two abrupt changes in neutron flux and temperature. Examination by transmission electron microscopy showed that HT9 retained its swelling resistance in spite of the somewhat complex flux and temperature history, reaching only about 0.3%. Based on this study only, it can not be determined whether the transient regime of swelling is still in progress or the steady-state swelling rate is being approached.

Acknowledgements

This research is supported by the Advanced Fuel Cycle Initiative (AFCI). The authors are indebted to M.B. Toloczko of Pacific Northwest National Laboratory for the information describing the irradiation conditions of the AC0-3 duct, as presented in Fig. 2 and Tables 2 and 3 and to W. Witherspoon who led the retrieval of this duct. A special acknowledgment is given to F. Goldner at DOE for making all this happen. We also thank T. Romero for remotely cutting the TEM specimens from the duct and J. Gan for sample preparation. We also acknowledge the staff of UNLV for the use of their electron beam facility.

References

[1] Proceedings of the Topical Conference on Ferritic Alloys for use in Nuclear Energy Technologies, AIME, 1984, p. 559.
[2] E.A. Little, D.A. Stow, J. Nucl. Mater. 87 (1979) 25.
[3] R.W. Powell, D.T. Peterson, M.K. Zimmerscheid, J.F. Bates, J. Nucl. Mater. 103–104 (1981) 969.
[4] G.R. Odette, J. Nucl. Mater. 155–157 (1988) 921.
[5] R.L. Klueh, K. Ehrlich, F. Abe, J. Nucl. Mater. 191–194 (1992) 116.
[6] A.G. Ioltukhovsky, V.P. Kondrat'ev, M.V. Leont'eva-Smirnova, S.N. Votinov, V.K. Shamardin, A.V. Povstyanko, T.M. Bulanova, J. Nucl. Mater. 233–237 (1996) 299.
[7] A. Hishinuma, A. Kohyama, R.L. Klueh, D.S. Gelles, W. Dietz, K. Ehrlich, J. Nucl. Mater. 258–263 (1998) 193.
[8] B. van der Schaaf, D.S. Gelles, S. Jitsukawa, A. Kimura, R.L. Klueh, A. Moslang, G.R. Odette, J. Nucl. Mater. 283–287 (2000) 52–59.
[9] R.L. Klueh, D.S. Gelles, S. Jitsukawa, A. Kimura, G.R. Odette, B. van der Schaaf, M. Victoria, J. Nucl. Mater. 307–311 (2002) 455.
[10] S. Jitsukawa, A. Kimura, A. Kohyama, R.L. Klueh, A.A. Tavassoli, B. van der Schaff, G.R. Odette, J.W. Rensman, M. Victoria, C. Petersen, J. Nucl. Mater. 329–333 (2004) 39.
[11] A. Kimura, R. Kasada, A. Kohyama, H. Tanigawa, T. Hirose, K. Shiba, S. Jitsukawa, S. Ohtsuka, S. Ukai, M.A. Sokolov, R.L. Klueh, T. Yamamoto, G.R. Odette, J. Nucl. Mater. 367–370 (2007) 60.
[12] D.S. Gelles, J. Nucl. Mater. 239 (1996) 99.
[13] D.S. Gelles, 12Cr-1Mo steel for fission and fusion applications, in: Proc. ASM Intern. Conf. on Ferritic Steels for High Temperature Applications, Warren, PA, October 1981, p. 197.
[14] D.S. Gelles, L.E. Thomas, Effects of neutron irradiation on microstructure in experimental and commercial ferritic alloys, in: Proc. AIME Topical Conf. on Ferritic Alloys for Use in Nuclear Energy Technologies, Snowbird, UT, June 1983, p. 559.
[15] D.S. Gelles, DOE/ER-0046/24 (1986) 43.
[16] D.S. Gelles, J. Nucl. Mater. 233–237 (1996) 293.
[17] F.A. Garner, D.S. Gelles, Neutron-induced swelling of commercial alloys at very high exposures, in: N.H. Packan, R.E. Stoller, A.S. Kumar (Eds.), Effects of Radiation on Materials: 14th International Symposium, ASTM STP 1046, vol. 2, American Society for Testing and Materials, Philadelphia, 1990, pp. 673–683.
[18] R.J. Puigh, F.A. Garner, Irradiation creep behavior of the fusion heats of HT9 and modified 9Cr-1Mo steels, in: N.H. Packan, R.E. Stoller, A.S. Kumar (Eds.), Effects of Radiation on Materials: 14th International Symposium, ASTM STP 1046, vol. 2, American Society for Testing and Materials, Philadelphia, 1990, pp. 527–536.
[19] F.A. Garner, R.J. Puigh, J. Nucl. Mater. 179–181 (1991) 577.
[20] M.B. Toloczko, F.A. Garner, C.R. Eiholzer, J. Nucl. Mater. 212–215 (1994) 604.
[21] M.B. Toloczko, F.A. Garner, J. Nucl. Mater. 233–237 (1996) 289.
[22] M.B. Toloczko, F.A. Garner, Variability of irradiation creep and swelling of HT9 irradiated to high neutron fluence at 400-600 °C, ASTM STP 1325, in: R.K. Nanstad, M.L. Hamilton, F.A. Garner, A.S. Kumar (Eds.), Effects of Radiation on Materials: 18th International Symposium, American Society of Testing and Materials, 1999, pp. 765–779.
[23] M.B. Toloczko, B.R. Grambau, F.A. Garner, K. Abe, Comparison of thermal creep and irradiation creep of HT9 pressurized tubes at test temperatures from 490 °C to 600 °C, in: S.T. Rosinski, M.L. Grossbeck, T.R. Allen, A.S. Kumar (Eds.), Proceedings of Symposium on Effects of Radiation on Materials, 20th International Symposium, ASTM STP 1405, American Society for Testing and Materials, West Conshohocken, PA, 2001, pp. 557–569.
[24] F.A. Garner, Irradiation Performance of Cladding and Structural Steels in Liquid Metal Reactors, Vol. 10A of Materials Science and Technology: A Comprehensive Treatment, VCH Publishers, 1994, pp. 419–543 (Chapter 6).
[25] J.J. Laidler, R.J. Jackson, Trans. ANS 49, 90.
[26] R.D. Leggett, L.C. Walters, J. Nucl. Mater. 204 (1993) 23.
[27] R.B. Baker, F.E. Bard, R.D. Leggett, A.L. Pintner, J. Nucl. Mater. 204 (1993) 109.
[28] D.S. Gelles, L.E. Thomas, in: Proceedings of the Topical Conference on Ferritic Alloys for use in Nuclear Energy Technologies, AIME, 1984, p. 559.
[29] P.L. Maziasz, R.L. Klueh, Void Formation and Helium Effects in 9Cr-1MoVNb and 12 Cr-1MoVW Steels Irradiated in HFIR and FFTF at 400 C, to be published in proceedings of the 14th International Symposium on the Effects of Radiation on Materials, held June 27–29, 1988, in Andover, MA.
[30] D.S. Gelles, R.M. Claudson, L.E. Thomas, Electron Microscopy 1990, vol. 4, San Francisco Press, San Francisco, 1990, pp. 844–845.
[31] S.I. Porollo, A.M. Dvoriashin, A.N. Vorobyev, Yu.V. Konobeev, J. Nucl. Mater. 256 (1998).
[32] A.M. Dvoriashin, S.I. Porollo, Yu.V. Konobeev, F.A. Garner, J. Nucl. Mater. 283–287 (2000) 157.
[33] N.I. Budylkin, E.G. Mironova, V.M. Chernov, V.A. Krasnoselov, S.I. Porollo, F.A. Garner, J. Nucl. Mater. 375 (2008) 359.
[34] F.A. Garner, M.B. Toloczko, B.H. Sencer, J. Nucl. Mater. 276 (2000) 123.
[35] E.A. Little, D.A. Stow, J. Nucl. Mater. 206 (1993) 324.
[36] B.H. Sencer, F.A. Garner, J. Nucl. Mater. 283–287 (2000) 164.
[37] Y. Katoh, A. Kohyama, D.S. Gelles, J. Nucl. Mater. 225 (1995) 154.
[38] D.S. Gelles, J. Nucl. Mater. 225 (1995) 163.
[39] F.A. Garner, D.S. Gelles, L.R. Greenwood, T. Okita, N. Sekimura, W.G. Wolfer, J. Nucl. Mater. 329–333 (2004) 1008.
[40] T. Okita, N. Sekimura, T. Sato, F.A. Garner, L.R. Greenwood, J. Nucl. Mater. 307–311 (2002) 322.
[41] T. Okita, W.G. Wolfer, T. Sato, N. Sekimura, F.A. Garner, Influence of composition, helium generation rate and dpa rate on neutron-induced swelling of Fe-15Cr-1Ni-0.25Ti alloys in FFTF at ~400 °C, in: 11th International Conference on Environmental Degradation of Materials in Nuclear Power Systems – Water Reactors, 2003, pp. 657–663.
[42] F.A. Garner, N.I. Budylkin, Yu.V. Konobeev, S.I. Porollo, V.S. Neustroev, V.K. Shamardin, A.V. Kozlov, The influence of dpa rate on void swelling of Russian austenitic stainless steels, in: 11th International Conference on Environmental Degradation of Materials in Nuclear Power Systems – Water Reactors, 2003, pp. 647–656.
[43] N.I. Budylkin, T.M. Bulanova, E.G. Mironova, N.M. Mitrofanova, S.I. Porollo, V.M. Chernov, V.K. Shamardin, F.A. Garner, J. Nucl. Mater. 329–333 (2004) 621.
[44] A.M. Dvoriashin, S.I. Porollo, Yu.V. Konobeev, F.A. Garner, J. Nucl. Mater. 329–333 (2004) 319.